PCCP

ROYAL SOCIETY OF CHEMISTRY

ARTICLE TYPE

Cite this: DOI: 10.1039/xxxxxxxxxx

ESI: Mechanisms of lipids extraction from skin lipid bilayers by sebum triglycerides

Anna Sofia Tascini,*[a] Massimo G. Noro,[b‡] John M. Seddon,[a] Rongjun Chen[c] and Fernando Bresme[a]

Received Date
Accepted Date

DOI: 10.1039/xxxxxxxxxx

www.rsc.org/journalname

Electronic Supplementary information of Mechanisms of lipids extraction from skin lipid bilayers by sebum triglycerides.

S1 Methods

S1.1 Construction of the SC bilayer

The SC membrane was constructed using the open source software Packmol[1] to place 288 SC lipid molecules in each of the two leaflets of a bilayer, symmetrically about the bilayer mid-plane. Packmol was used to place the lipid and water molecules inside rectangular regions with a random distributions. To better reproduce the bilayer structure, the top oxygen atoms of the OH group of the hydrophilic head groups and the terminal carbon atom of the longest acyl tail of each lipid molecule were constrained to lie above or under predefined planes (as shown in Fig. S1). A distance of 1.4 Å between molecules was adopted to avoid overlapping between them. The system was then equilibrated in water, following the procedure described in ref. 2: *i.e.* the system was run for 5 ns with the stratum corneum molecules fixed (to hydrate the bilayer properly), and then for 2 ns with only the terminal methyl group on all the lipid tails frozen, so that the rest of the molecules reorient themselves to accommodate the water environment. A further 50 ns NPT equilibration was run before joining the SC bilayer to the TG slabs. See the main paper for details on the simulation parameters.

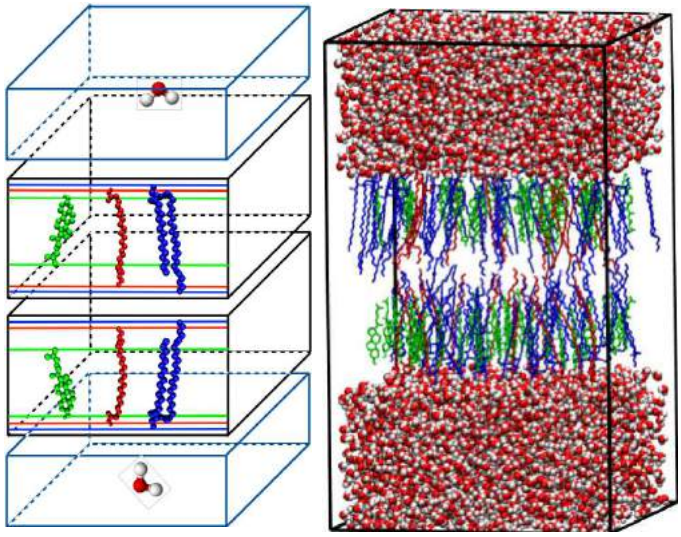

Fig. S1 The scheme on the left shows the constraints adopted in Packmol[1] to create the bilayer configuration. The output configuration is shown on the right.

S1.2 Tracking the extraction mechanisms

The numbers of TG insertions and lipid extractions were obtained through the method explained below, which was implemented in an in-house code.

In order to identify the boundaries of the lipid bilayer one atom of each lipid type is considered to determine the position of the lipid head groups. Specifically we used O21 for CR2, O6 for CHO, O1 for FFA (see Fig. 3 in the main paper for labels). The z positions of the lipid head group atoms are histogrammed (see blue line in Fig. S2) and the value of the two maxima in the histograms are used to define the edges of the bilayer (see dashed lines). The bilayer midpoint is defined as halfway between these values.

Once the bilayer midpoint has been calculated from the histograms, two slices through the bilayer, parallel to the xy plane, are defined at a specified height, d_{SLICE}, above and below the bilayer midpoint. The height, d_{SLICE}, is chosen so that the slice is entirely within one of the leaflets of the bilayer, just below the head group maxima, and does not include the bilayer surface. The slice thickness must be larger than the largest bond length for molecules within the bilayer to ensure that if the slice passes though a molecule, at least one of the molecules atoms are within the slice volume. A graphical example of the definition of the

[a] *Department of Chemistry, Imperial College London, UK; E-mail: ast14@ic.ac.uk, fbresme@imperial.ac.uk*
[b] *Unilever R&D Port Sunlight, Quarry Road East, Bebington, Wirral, CH63 3JW, UK.*
‡ *Present address: Science and Technology Facility Council (STFC), Daresbury Laboratory, Sci-Tech Daresbury, Keckwick Lane, Daresbury, Warrington, WA4 4AD*
[c] *Department of Chemical Engineering, Imperial College London, UK.*

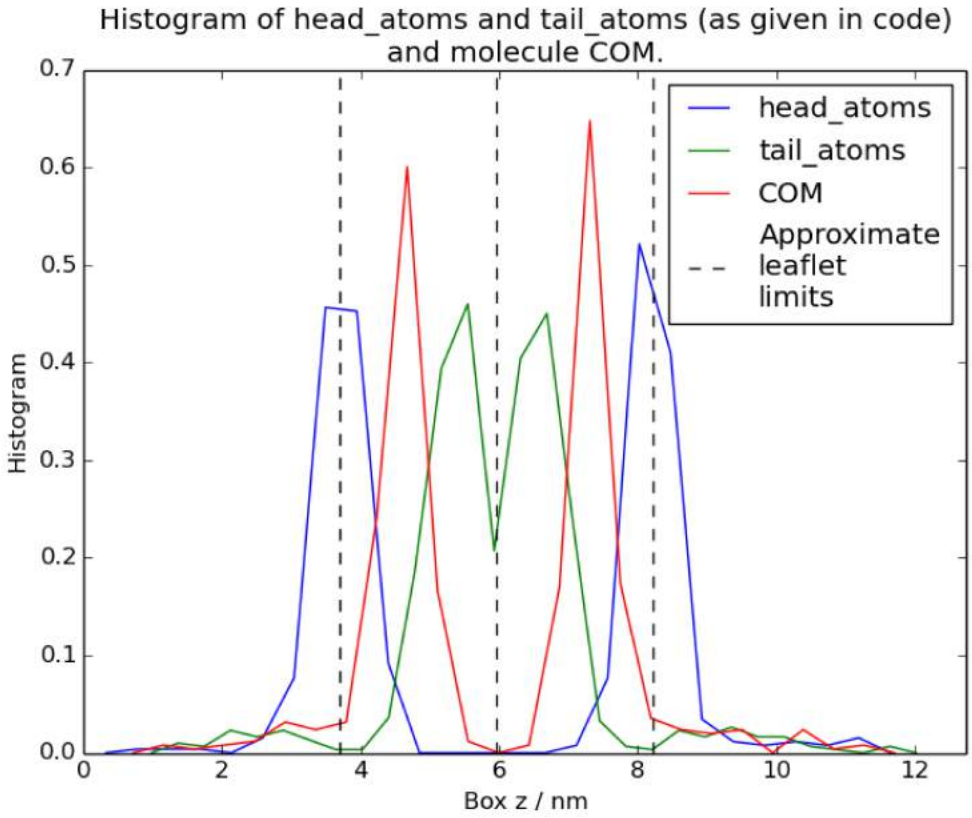

Fig. S2 a) Histogram of lipid subgroups, namely head groups (in blue), tails (in green) and centre of mass (red). The leaflets limits and the bilayer mid-plane, estimated by the code, are shown with dashed lines.

slices is shown in Fig. 2 in the main paper.

The atoms inside each slice are recorded (as shown in Fig. 2 in the main paper) and individual molecules are assigned to one of the two leaflets or to the TG phase by checking whether at least one of their atom was inside or outside the slices. Specifically, if a SC lipid molecule does not have atoms in either of the two slices, it is assigned as being outside the bilayer and one extraction event is counted. If a TG molecule is found to be in one of the slices it is considered to be anchored to the bilayer. For molecules with more than one chain, *i.e.* TG and CR2, each chain is considered separately in order to assign part of the molecule to the bilayer or the TG phase, based on the positions of the atoms in the chain. The resulting configuration of TG or CR2 molecules is then determined by considering the relative assignment of the individual chains.

In TG anchoring the three fatty acid chains are treated separately to check whether TG molecules insert with one, two or three chains and assess the conformation of the inserted molecule. The TG atoms are assigned to the three chains as specified in Fig. S3.

For the CR2 split event, *i.e.* when a CR2 molecule has the two chains widely spread forming an angle of $\sim 180^\circ$ with one of the chain in the bilayer and the other one in the TG phase, it is distinguished whether the chain within the slice is the sphingosine chain or the fatty acid chain. The CR2 atoms are assigned to the chains as shown in Fig. S3. A full CR2 extraction is counted when all the atoms from both chains are found outside the slices.

S1.3 Assessing the area per lipid

The atom coordinates within the slices were used as generators for the Voronoi tessellation method in two dimensions (see Fig. 2 in the main paper). To any atom was assigned its closest region of the 2D space.

Once the Voronoi tessellation was obtained, the area of a planar non-self-intersecting polygon with vertices (x_1,y_1), ..., (x_n,y_n) was calculated by[3]

$$A_P = \frac{1}{2}\left(\begin{bmatrix} x_1 & x_2 \\ y_1 & y_2 \end{bmatrix} + \begin{bmatrix} x_2 & x_3 \\ y_2 & y_3 \end{bmatrix} + \cdots + \begin{bmatrix} x_{n-1} & x_n \\ y_{n-1} & y_n \end{bmatrix} + \begin{bmatrix} x_n & x_1 \\ y_n & y_1 \end{bmatrix}\right). \tag{S1}$$

The area per lipid of each molecule (i) was obtained by averaging the contributions of the single polygons, A_P, as

$$A_{L,i} = \langle \frac{\sum_{N_L} A_P}{N_L} \rangle, \tag{S2}$$

where N_L is the number of molecules of specie L found within the slices and $\langle ... \rangle$ represents a time average.

S2 TG penetration

We observed that a number of TG molecules anchor to the SC bilayer via their acyl chains. The number of insertion events *vs.* time in the top and bottom leaflets is displayed in Fig. S4. We

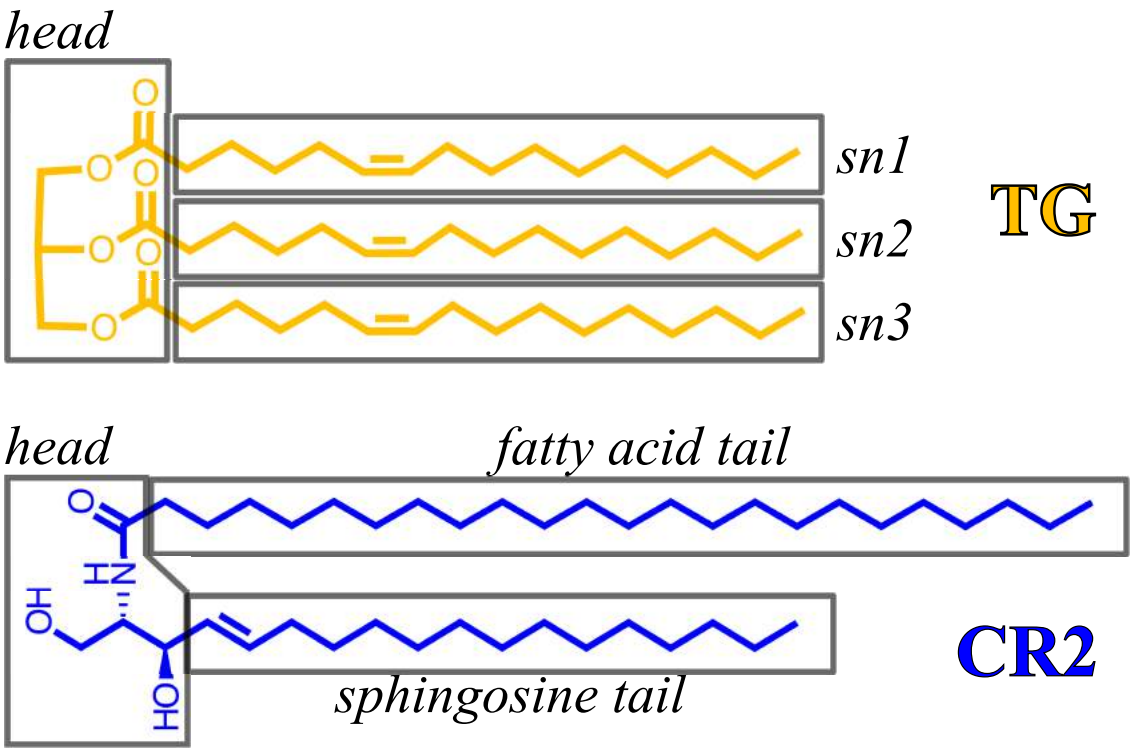

Fig. S3 Top) The atoms of a TG molecule were separately assigned to one of the three fatty acid chains (*sn1*, *sn2* or *sn3*) or to the glycerol group (*head*). Bottom) Atoms in a CR2 molecule are divided in *head* group atoms, *fatty acid* tail and *sphingosine* tail. The atom assignment is shown with grey rectangular boxes.

determine the anchoring via the procedure explained in the main paper and subsection S1.2.

The result shows that the number of insertions stabilises to ≈ 20 insertions in each leaflet, following a long transient process that spans $\approx 1.1\,\mu$s. The most common type of interdigitation for TG molecules ($\approx 89.7\%$ of the events) is the insertion of one of the three tails, as displayed in the top graph of Fig. S4 and in Fig. 4 in the main paper. A smaller fraction of TG lipids penetrates in the bilayer with two ($\approx 7.7\%$) or three ($\approx 2.6\%$) chains (see middle and bottom graphs of Fig. S4 respectively).

We estimated the preferred conformations of the TG molecules from the three angles between the triglyceride chains (θ_{12}, θ_{23} and θ_{13}). The direction of the chains were defined as the vectors between one of the carbon atoms of the glycerol group and the corresponding 6-*cis* carbon on each chain (see TG structure in Fig. S3). θ_{12}, θ_{23} and θ_{13} were, then, computed as the angles between the corresponding vectors ($\vec{V}_1$, $\vec{V}_2$ and $\vec{V}_3$), as

$$\theta_{12} = \arccos\left(\frac{\vec{V}_1\cdot\vec{V}_2}{\left|\vec{V}_1\right|\left|\vec{V}_2\right|}\right),$$
$$\theta_{23} = \arccos\left(\frac{\vec{V}_2\cdot\vec{V}_3}{\left|\vec{V}_2\right|\left|\vec{V}_3\right|}\right), \qquad \text{(S3)}$$
$$\theta_{13} = \arccos\left(\frac{\vec{V}_1\cdot\vec{V}_3}{\left|\vec{V}_1\right|\left|\vec{V}_3\right|}\right).$$

The energetically favourable regions of TG conformations, expressed in terms of the three angles θ_{12}, θ_{23} and θ_{13} were linked to four different shapes: the tuning fork, the propeller, the chair and the trident, using the criteria discussed in ref. 4.

The analysis involved an averaging of the TG conformations over the last $0.1\,\mu$s of the trajectory. Fig.5 in the main paper shows the 3D distributions of TG conformations as a function of the three angles described by the mutual orientation of the chains: θ_{12}, θ_{23} and θ_{13} for anchored TG molecules (bottom graph) and non-anchored TG molecules (top graph).

As noted in ref. 4, the preferred conformation of the TG molecules is the tuning fork shape, with the two external chains ($\vec{V}_1$ and $\vec{V}_3$) pointing in the same direction and opposite to the direction of the central ($\vec{V}_2$) chain.

The number of trident conformations in the non anchored TG molecules ($\approx 24\%$) is higher than in the pure TG phase ($\approx 15\%$[4]). This increase is connected to the presence of the SC bilayer, which induces a rearrangement of the TG lipids. This observation is consistent with the structure of the TG molecules at the water-TG interfaces, where the trident conformation was also observed. We found a preference for the tuning fork conformation in the molecules anchored to the bilayer too. These molecules anchor to the bilayer by inserting the middle chain (direction $\vec{V}_2$). Other conformations, namely the propeller and the chair, are enhanced significantly with respect to the population observed among the non-anchored molecules, while the number of trident configurations is reduced significantly (see % in the main paper). The on-off fluctuations in Fig. S4-bottom suggest that the third chain

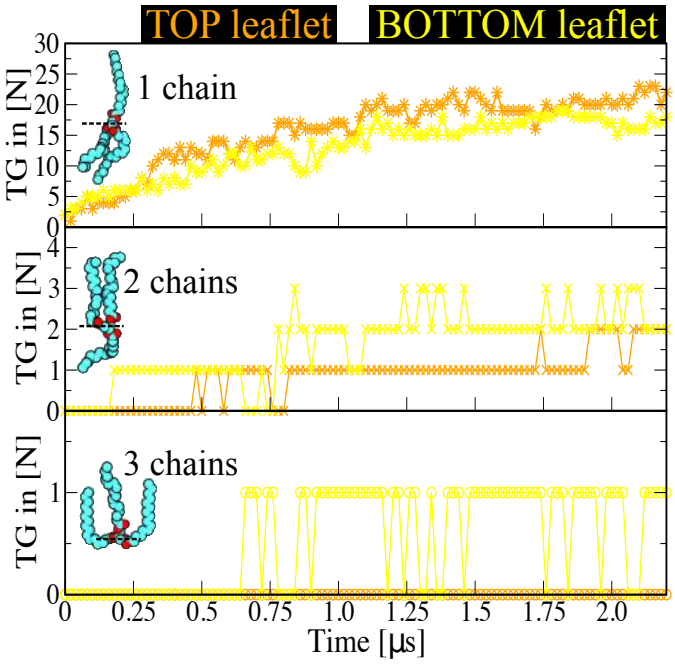

Fig. S4 Number of penetrating TG molecules vs time in the bottom (yellow curves and symbols) and top (orange curve and symbols) leaflet, with one (top graph), two (middle graph) or three (bottom graph) chains.

might be entering the bilayer only superficially, comparing this case to the insertion of only 2 chains.

S2.1 TG clustering criteria

The TG clusters were determined following the methodology described in ref 4. The open source software voro++[5] was used to decompose the TG configuration into 3D Voronoi cells and to list neighbouring particles, defined as particles whose Voronoi cells share a common face. To capture the basic structure of the TG molecule, the head group (i.e. the glycerol moiety) was simplified by combining all of the head group atoms together and representing them by a single point located at the position of the central glycerol carbon atom. The tessellation was then performed using this head group point and the carbon atoms of the acyl tails. Clusters were defined by grouping together the head group Voronoi polyhedra which shared a face. The method was used to quantify the size and the shape of the TG clusters. In Fig. S5 we show the resulting clusters at $t = 2\mu$s, using different colours.

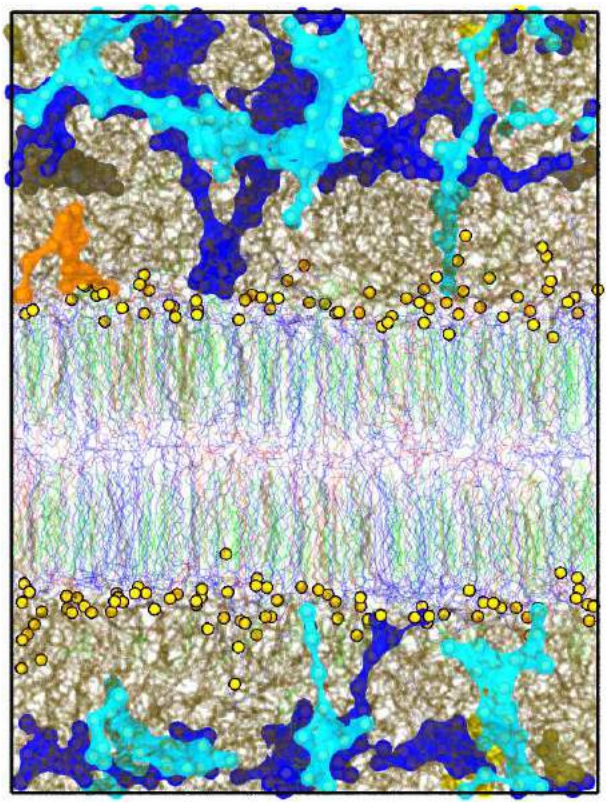

Fig. S5 Representative snapshot from the simulation where the TG head groups (GLY) clusters are joined together using the VMD[6] drawing mode "Surf" with probe radius $= 2.4$Å[7] and highlighted in different colours (blue, light-blue, orange, yellow and grey). The TG head groups are represented with yellow spheres located in the central carbon atom of the glycerol group and the tails as brown sticks. The SC lipids are represented with coloured lines (with the same colour code as Fig. 1 in the main paper).

S3 CR2 splitting

We have reported in the main paper that CR2 molecules rarely leave the bilayer, with some molecules ($\approx 11\%$) found in an arrangement where the two chains form an angle of $\approx 180^\circ$. We have quantified the number of CR2 splitting events *vs.* time (see Fig. S6a), by differentiating between conformations where the chain detaching from the bilayer is the free fatty acid (blue circles and inset 1) or the spinghosine (light-blue diamonds and inset 2). We find that the the free fatty acid motif is three times more likely to be involved in the splitting event. Due to the strong asymmetry of the acyl chains, the longer C24 chain tends to bend either in the space between the two leaflets or in the head-group region[8]. When it adopts the latter conformation (*i.e.* C24 tails bending in the interfacial region) the splitting event is more likely to occur, with the C24 chain interdigitating into the oil layer, in the space occupied by the TG acyl chains. Fig. S6b shows snapshots illustrating the dynamics of the splitting event for two CR2 molecules, from the top (above the time line) and bottom (below the time line) leaflets. In both cases the C24 chain first bends at the interface and then goes to the TG phase.

The existence of extended configurations for ceramide molecules, such as the one observed here at the TG interface, has been previously noted in studies involving stacks of lipid bilayers[9–12]. In those cases the bilayers in the middle of the stacks are in an anhydrous environment, as in our simulations. Moore *et al.* [12] reported, using coarse grained models, that in a stack of ceramide bilayers the percentage of ceramide molecules found in extended conformations increases in the inner leaflets where the lipid molecules are not in contact with water.

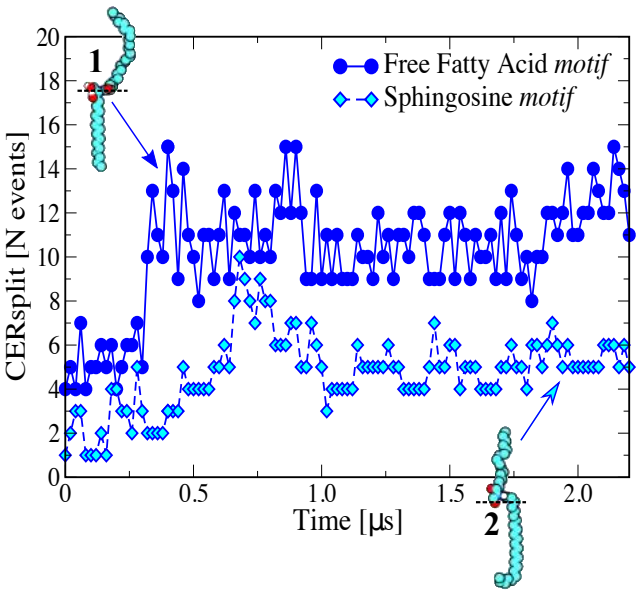

(a) CR2 splitting

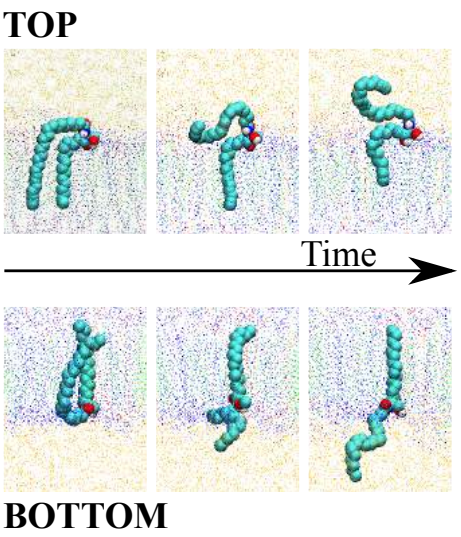

(b) C24 split dynamics

Fig. S6 (a) Number of CR2 splitting *vs.* time. The blue circles correspond to the number of CR2 split with the C24 tail in the oily phase; the light-blue diamonds correspond to the case where the C18 tail is in the oily phase. Inset 1 and 2 show two representative CR2 splitting events in the top leaflet. (b) Two examples of C24 splitting in the sebum oil via 3 consecutive snapshots for one molecule in the top (above the time line) and bottom (below the time line) leaflets.

S4 CHO and FFA head group distributions and 1D energy profiles

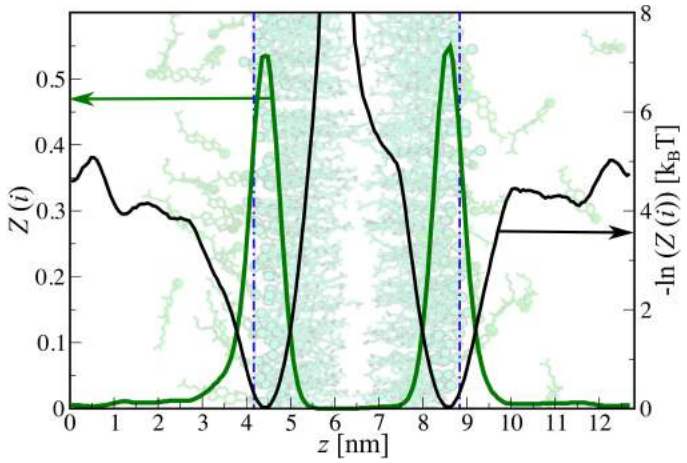

Fig. S7 Distribution of the cholesterol head groups (atom O6) along z, $Z(i)$, on the left-hand side axis and free energy in k_BT units on the right-hand side axis.

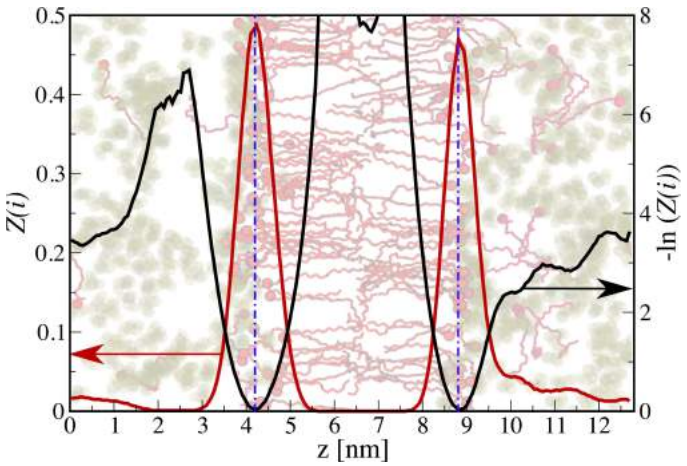

Fig. S8 Distribution of the free fatty acid head groups (atom O1) along z, $Z(i)$, on the left-hand side axis and free energy in units of k_BT on the right-hand side axis. A representative system configuration, at $t = 2.2\mu$s, is shown in the background of the plot showing the FFA molecules and the glycerol group distribution in the TG phase.

The CHO molecules were found to preferentially leave the bilayer through a flip-flop like event, where the CHO molecules reverse their orientation before adsorbing at the SC bilayer. These events can be tracked with our microsecond simulations and the free energy differences can be quantified too from $\Delta G = -k_BT \ln(\rho(z)/\rho_0)$, where ρ_0 is a reference density which we take at the minimum position corresponding to the maximum at $z \sim 4$nm. We show in Fig. S7 the density profile of the CHO head group (oxygen, O6) obtained from the analysis of a trajectory spanning $1.5\,\mu$s.

The profile features two main peaks which indicate the preferred location of the head group of CHO in the SC bilayer. The position of the peaks indicates that the CHO head group is preferentially located below the TG-SC interface (see blue dashed line in Fig. S7 for a reference of the position of the interface). This result is consistent with previous simulation studies[13]. Most of the CHO molecules extracted from the bilayer adsorb at the TG-SC interface. This leads to a shallower gradient for the energy profile on the TG side.

Fig. S8 shows the distribution of FFA O1 atoms along z and the corresponding free energy profile. In the region of the graph where there is an absorption barrier and consequently a smaller number of events, there is also a gap in the glycerol group network, which could explain the asymmetry in the free energy distribution as discussed in the main text. This is probably due to the time required for TG molecules to rearrange themselves and assume the percolating network conformation.

S5 Bilayer Stability

A key question in understanding the interaction between TG and the SC bilayer is whether the structure of the main components of the sebum oil is able to destroy the integrity of the SC bilayer. The effect of monoglycerides and fatty acids on the integrity of pure CR2 lipid bilayers in water has been the subject of a recent publication by Akinshina *et al.* [14]. The authors found the degree of unsaturation of the acyl chain to play a crucial role in determining the bilayer integrity, ranging from complete stability against *trans*-unsaturated oils to loss of structure in presence of a single *cis*-double bond oil with an oil content within the bilayer of about 50 - 65%. Specifically, sapienic acid, the most abundant free fatty acid present in sebum [15] is characterised by a single double bond at the 6th position from the carboxyl end, which might have an impact on the SC lipid bilayer.

S5.1 SC lipid extraction

To estimate whether the sebum triglycerides would progressively cause a loss of structure in the SC bilayer, the percentage of lipids remaining in the bilayer, $\%N_{SC}$, as a function of time was evaluated.

The number of lipids in the bilayer was obtained through the method described in section S1.2. $\%N_{SC}$ is reported in Fig. S9 for each lipid species. As mentioned before, even after $2\,\mu$s, the total number of extracted CR2 is just $\approx 2\%$, and $\approx 15\%$ for CHO and FFA, with most of the lipid molecules therefore remaining in the bilayer. In addition, after a first faster reduction for $\approx 0.75\,\mu$s, the lipid percentage levels off towards a constant value (similarly to what was observed for TG insertion, see Fig. S4.

In the inset of Fig. S9, the number of extractions *vs.* time is tracked, distinguishing the number of events in the top (solid lines) and bottom (asterisks) leaflet. The number of CR2, CHO and FFA events is slightly asymmetric in the two leaflets, with the number of CR2 splits and FFA escapes being larger in the top leaflet than the bottom one and *vice-versa* for the CHO extractions. This could be due to some initial asymmetry in the distribution of the lipids in the top and bottom leaflets. The network of TG head groups and the insertion of the TG chains in turn could also locally induce modification in the lipid conformation and drive new extraction events.

After $1\,\mu$s at the extraction plateau the composition of the bilayer is very similar to the initial one (CR2:CHO:FFA=2:2:1 molar ratio) with an enrichment in TG and a small reduction in the concentration of FFA and CHO. The fractional concentration of TG chains within the bilayer is equivalent to ≈ 0.1 TG chains per SC lipids. Therefore, despite the presence of a *cis*-double bond, the small concentration of TG chains able to penetrate the bilayer is not enough to cause a loss of integrity in the SC bilayer, in agreement with the prediction of Akinshina *et al.* [14].

S5.2 Area per Lipid *vs.* time

The evolution of the area per lipid, A_L, *vs.* time can also be employed as a measure of the bilayer stability. A_L of the different lipids was derived via the Voronoi tessellation method (see section S1.3) and shown in Fig. S10 and Table S1.

Lipid	A_L [nm^2]	Err [nm^2]
CR2	0.40356	0.07414
CHO	0.35226	0.06544
FFA	0.21793	0.04405
TG	0.25988	0.10843

Table S1 Mean value and standard deviation of A_L measurements. The data are averaged over the simulation length. The error represent the standard deviation of the measurement via Voronoi tessellation method (see section S1.3).

All the values of area per lipid, reported in Fig. S10, stay constant over the period of the simulation and their value is very close to the one measured for SC lipids in water. This indicates that insertion of TG compensates for the extraction events and suggests that CR2, CHO and FFA maintain their favoured area per lipid, without big alterations of the lipid packing caused by the interdigitation mechanisms, supporting the hypothesis of bilayer stability. Remarkably, the value obtained for the area per lipid of CR2 ($\approx 0.4\,$nm^2) is in agreement with the experimental value obtained by X-ray experiments [16], confirming the accuracy of the proposed forcefield in reproducing experimental data. The small variations of this value in the first $0.75\,\mu$s are caused by the CR2 splitting events happening during the equilibration stage.

The TG area per lipid is very similar to the FFA area per lipid. This is due to the fact that TG molecules preferentially penetrate the bilayer with a single chain. The slightly higher value is due to the presence of a double bond in the TG chains and to the existence of a few TG molecule penetrating with 2 or 3 chains.

S5.3 Hydrogen bonding

Hydrogen bonding is another key property for characterising the structural features of SC bilayers interacting with water, oils or small molecules and affects the bilayer stability [8,14,17–19]. CR2 molecules in single component bilayers form a strong network of hydrogen bonds with other lipids and water, which leads to the formation of hexagonal packing [8], making the bilayer rigid and difficult to permeate. The CR2 molecules can in fact be hydrogen bond acceptors and donors at the same time at three different sites. As previously shown by simulations [13,20] and experiments [21], the addition of CHO and FFA to the bilayer, lipids with just 1 acceptor and 1 donor site each, results in more flexible systems, where long-range hexagonal arrangement is not observed. The effect of TG has been investigated by calculating the hydrogen bonding for the lipid species in the system via the GROMACS tool `g_hbond` with default parameters for the definition of hydrogen bonds, *i.e.* a hydrogen bond is counted for distances between the donor and acceptor atom lower than 0.35 nm and acceptor-donor-hydrogen angles within 30°.

Results are presented in Fig. S11 and Table S2. The graph in Fig. S11 shows the number of hydrogen bonds (normalised by the total number of lipids in the bilayer, $N_{SC} = 576$) *vs.* time, highlighting the intra-bilayer (SC-SC) and extra-bilayer (SC-TG) contributions. Interestingly, the overall impact of TG on the SC lipid

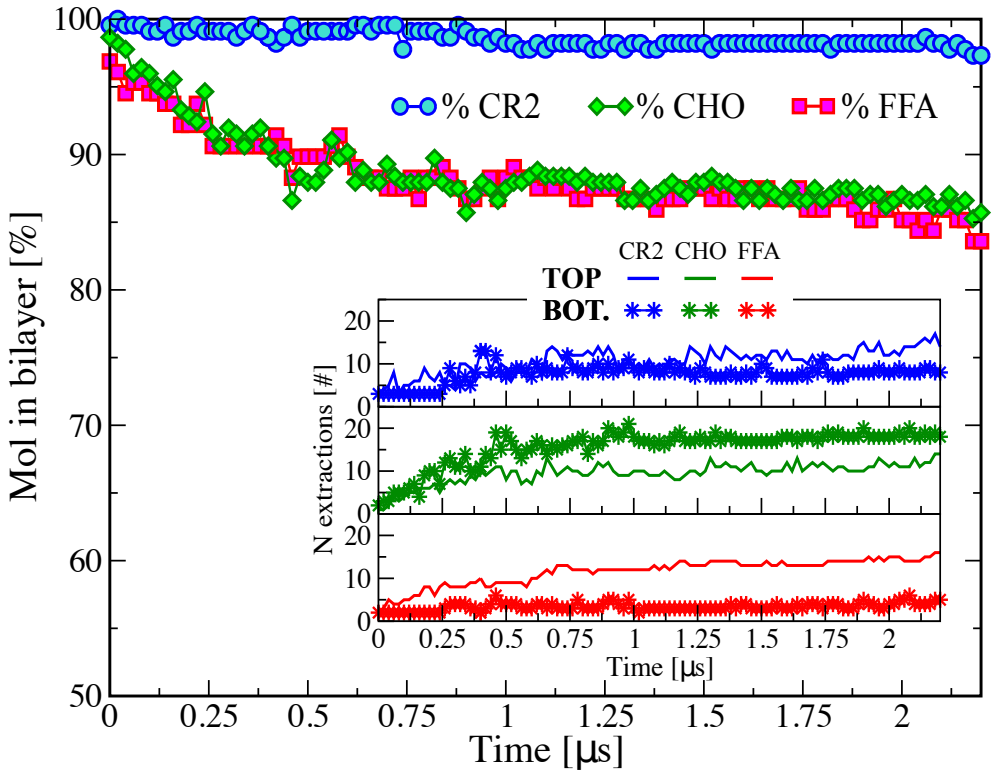

Fig. S9 Main) Percentage of lipid remaining in the bilayer *vs.* time, blue circles refer to CR2 molecules, green diamonds to CHO and red square to FFA. Inset) Number of extraction event *vs.* time for the three lipid species. From top to bottom: CR2, CHO and FFA. The N of events in the top leaflets are represented with a solid line and in the bottom with asterisks.

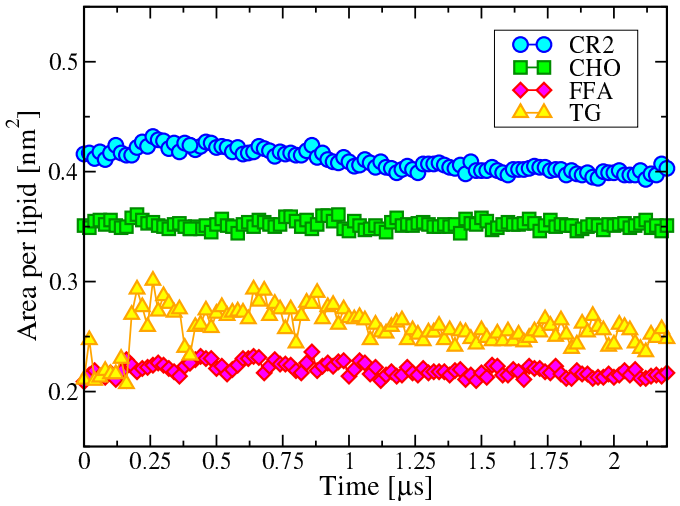

Fig. S10 Area per lipid *vs.* time for SC and sebaceus lipids, the different lipid contributions are highlighted with different colours and symbols, as specified in the legend. Error bars were not included in the plot for clarity, see Table S1 for uncertainty in the measurements.

bilayer is a slight increase in the total number of hydrogen bonds (purple curve). The rate of reduction in the number of hydrogen bonds within the SC lipids is in fact lower then the rate of growth of TG-SC hydrogen bonds. This might be related to the insertion of TG molecules into the bilayer, with a consequent reorganisation at the interface allowing closer contact and better alignment between donor groups of SC lipids and TG acceptors. The pie charts on the right of Fig. S11 show the contributions of the different lipid species to the total hydrogen-bonding, averaged over the last 10 ns of the simulation. Within the SC the main contribution to hydrogen bonding is the CR2 molecules bonding between themselves and other SC lipids ($\approx 93\%$ of the total hydrogen bonding involves a CR2 molecule). Looking at the SC-TG hydrogen bonding, one can observe that a significant amount of FFA and CHO molecules are hydrogen bonded with TG molecules, suggesting that in addition to the interfacial hydrogen bonds, some of these interactions involve the extracted molecules, dispersed in the TG phase. Table S2 shows the total number of hydrogen bonds per molecules, $N_{HB(i)}$, normalised by the number of lipids of the observed species (in bracket, where i is CR2, CHO and FFA respectively). Interestingly, FFA molecules tend to preferentially form hydrogen bonds with TG acceptors, confirming the interaction between the OH group of FFA and TG glycerol group as a pathway for the escape of FFA.

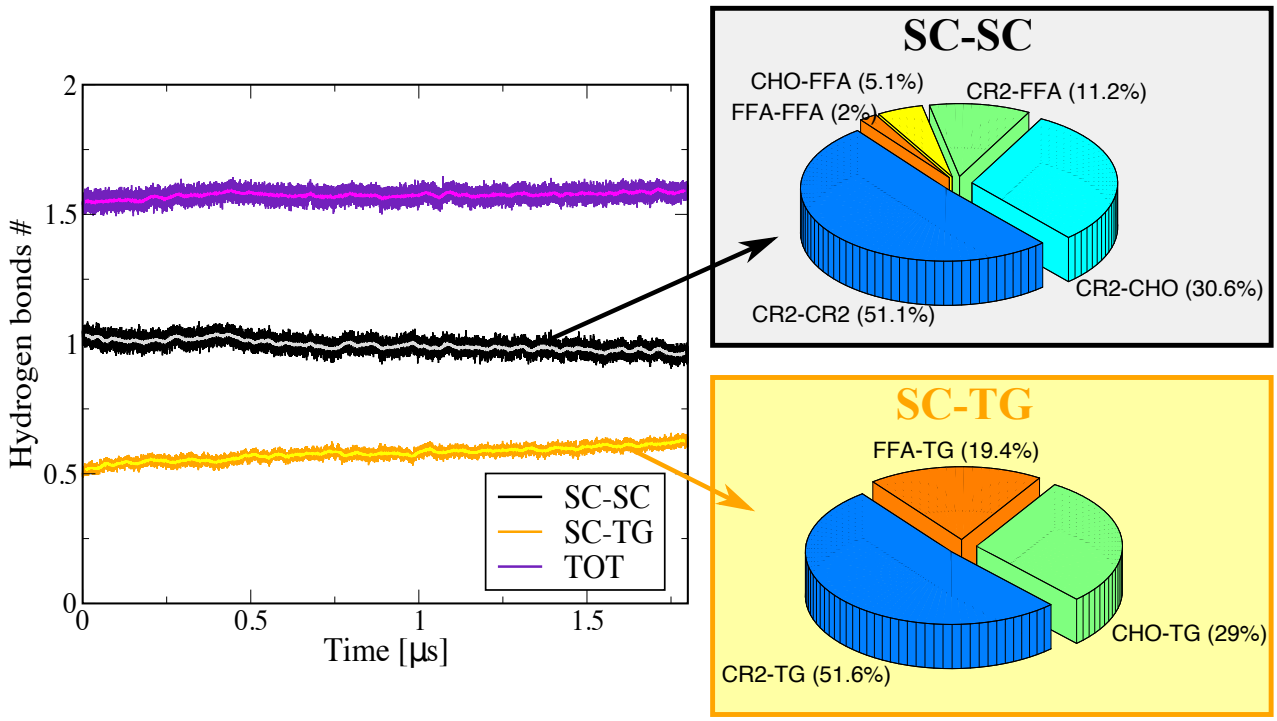

Fig. S11 Left) Number of hydrogen bonding per lipid *vs.* time. The intra-bilayer (SC-SC) and extra-bilayer (SC-TG) contributions are represented separately. Right) Lipid contribution (expressed as %) to SC-SC h-bond (top square) and SC-TG h-bond (bottom square).

	CR2	**CHO**	**FFA**
	$\mathbf{N_{HB(CR2)} = 3.13}$	$\mathbf{N_{HB(CHO)} = 1.45}$	$\mathbf{N_{HB(FFA)} = 1.31}$
CR2	40.6%	51.7%	35.1%
CHO	24.0%	0.0%	19.1%
FFA	8.9%	15.2%	4.6%
TG	26.5%	33.1%	41.2%

Table S2 Number of hydrogen bonds, $N_{HB,(i)}$, for SC lipid type: CR2, CHO and FFA. The proposed values are normalised with the total number of lipid of type *i* in the bilayer. The percentages show how the total number of hydrogen bonds is distributed among the different contributions.

References

1 L. Martinez, R. Andrade, E. G. Birgin and J. M. Martínez, *Journal of Computational Chemistry*, 2009, **30**, 2157–2164.

2 C. Das, M. G. Noro and P. D. Olmsted, *Biophysical Journal*, 2009, **97**, 1941–1951.

3 D. Zwillinger, *CRC Standard Mathematical Tables and Formulae*, 2003, p. 367.

4 A. S. Tascini, M. G. Noro, R. Chen, J. M. Seddon and F. Bresme, *Phys. Chem. Chem. Phys.*, 2018, **20**, 1848–1860.

5 C. H. Rycroft, *Chaos*, 2009, **19**, 041111.

6 W. Humphrey, A. Dalke and K. Schulten, *Journal of Molecular Graphics*, 1996, **14**, 33–38.

7 A. Varshney, F. P. Brooks and W. V. Wright, *IEEE Computer Graphics and Applications*, 1994, **14**, 19 – 25.

8 R. Notman, W. K. den Otter, M. G. Noro, W. J. Briels and J. Anwar, *Biophysical Journal*, 2007, **93**, 2056–2068.

9 L. Norlén, *Journal of Investigative Dermatology*, 2001, **117**, 830–836.

10 D. Kessner, A. Ruettinger, M. A. Kiselev, S. Wartewig and R. H. Neubert, *Skin Pharmacology and Physiology*, 2008, **21**, 58–74.

11 M. A. Kiselev, *Crystallography Reports*, 2007, **52**, 525–528.

12 T. C. Moore, C. R. Iacovella, R. Hartkamp, A. L. Bunge and C. McCabe, *Journal of Physical Chemistry B*, 2016, **120**, 9944–9958.

13 A. Del Regno and R. Notman, *Physical Chemistry Chemical Physics*, 2018, **20**, 2162–2174.

14 A. Akinshina, C. Das and M. G. Noro, *Phys. Chem. Chem. Phys.*, 2016, **18**, 17446–17460.

15 A. Pappas, *Dermato-Endocrinology 1:2,*, 2009, **1**, 72–76.

16 B. Dahlén and I. Pascher, *Chemistry and Physics of Lipids*, 1979, **24**, 119–133.

17 M. I. Hoopes, M. G. Noro, M. L. Longo and R. Faller, *Journal of Physical Chemistry B*, 2011, **115**, 3164–3171.

18 C. Das, P. D. Olmsted and M. G. Noro, *Soft Matter*, 2009, **5**, 4549–4555.

19 R. Notman and J. Anwar, *Advanced Drug Delivery Reviews*, 2013, **65**, 237–250.

20 C. Das, M. G. Noro and P. D. Olmsted, *Soft Matter*, 2014, **10**, 7346–7352.

21 J. A. Bouwstra and G. S. Gooris, *The Open Dermatology Jour-*

nal, 2010, **4**, 10–13.